propylene is not observed for the same reaction conditions on Ir(110)-(1×2), there is no evidence to suggest that a different intermediate is involved [i.e., there is ample evidence that the (110)-(1×2) surface possesses a greater specific activity for hydrogenation reactions]. The hydrogenolysis of cyclopropane was found to be qualitatively different from the hydrogenolysis of propane.[25] In particular, for cyclopropane on both surfaces, there was no variation in the apparent reaction kinetics over the entire temperature range investigated ($T \simeq 400$–600 K). This difference between cyclopropane and propane is due to the irreversibility of forming the adsorbed intermediate from cyclopropane. The observation of the production of ethylene on Ir(111) from the hydrogenolysis channel, coupled with precedents from organometallic chemistry,[31,32] suggests that the adsorbed intermediate is a mononuclear metallacycle butane. The lack of the observation of ethylene on Ir(110)-(1×2) does not exclude the possibility that this mechanism is dominant on both surfaces.

The hydrogenation of methylcyclopropane on both the Ir(111) and Ir(110)-(1×2) surfaces was found to be dominated by the production of *n*-butane for the reaction conditions considered here. This result was interpreted qualitatively by invoking parallel reaction mechanisms for the production of *n*-butane and isobutane, with the *n*-butane channel exhibiting a higher apparent activation energy and, thus, dominating at the relatively high temperatures. Different apparent reaction orders in P_{HC} and P_{H_2} for the production of *n*-butane compared to isobutane suggest that different intermediates (mechanisms) may be involved for the two hydrogenation pathways. We suggest that a π-allylic species may be involved in the reaction channel that produces *n*-butane and "linear" butenes, whereas a 1,3 di-σ-bonded intermediate is probably associated with the production of isobutane. The hydrogenolysis of methylcyclopropane was found to be similar to that found for cyclopropane on both surfaces. The observation of the production of propylene on the Ir(111) surface is consistent with the participation of a metallacycle butane in the hydrogenolysis channel. The selectivity difference observed between the two surfaces for the major hydrogenolysis channels would appear to support this mechanism. In particular, the absence of ethane in the major hydrogenolysis channel on the Ir(111) surface can be explained on a stereochemical basis if metallacycle butane formation proceeds through an edge complex[31] i.e., the presence of the methyl group prevents activation of the C_1–C_2 bond in methylcyclopropane by the coordinatively more saturated C_3 atoms of the Ir(111) surface.

Finally, the Ir(110)-(1×2) surface was found to possess a greater specific activity with respect to the Ir(111) surface for the hydrogenation of propylene. This observation, coupled with a number of others, implies a greater specific activity of the Ir(110)-(1×2) surface for hydrogenation reactions. One simple explanation for these observations is that the hydrogen adatom concentration is greater on the Ir(110)-(1×2) surface due to the presence of a previously identified,[23,24] higher binding energy adstate for hydrogen on this surface.

Acknowledgment. This work was performed at Sandia National Laboratories and supported by the U.S. Department of Energy under Contract DE-AC04-76DP00789. We acknowledge the partial support of the Office of Basic Energy Sciences, Division of Chemical Science (D.W.G.), and National Science Foundation Grant No. CHE-8617826 (W.H.W.).

Registry No. Ir, 7439-88-5; cyclopropane, 75-19-4; methylcyclopropane, 594-11-6; propylene, 115-07-1.

Laser-Induced Activation of Methane at Oxide Surfaces: A Probe of Radical–Surface Interactions

Basseera A. Sayyed and Peter C. Stair*

Department of Chemistry, Northwestern University, Evanston, Illinois 60208 *(Received: March 17, 1989; In Final Form: June 12, 1989)*

C–H bond activation was studied via pulsed laser irradiation of oxides in a methane atmosphere. Carbon monoxide was the major product observed at low power densities and room temperature. Significant amounts of C_2 products, ethane, ethylene, and acetylene were formed. CO, C_2H_6, C_2H_4, and C_2H_2 are assigned as primary products of the reaction. Laser-induced methane activation produces $^{\bullet}CH_3$ and $:CH_2$ radical species in the gas phase via a plasma mechanism and is utilized as a tool to study radical–oxide surface interactions. These reactions are surface sensitive as evidenced by the changes in conversion and product selectivity as a function of oxide pretreatment and oxides used.

Introduction

Methane activation is a subject of considerable scientific and practical interest. This is mainly due to the large abundance of methane, a major component of natural gas present in remote areas of the world, and the enormous economic gains possible in converting it to easily transportable liquid fuels. In general, thermal routes to methane activation have been inefficient due to the endothermicity of the process.[1,2] Commercial processes presently used to convert methane to synthetic crude and gasoline distillate usually involve steam reforming to produce synthesis gas as an intermediate step.[2,3] The substantial capital investments required to implement this process have motivated research into the possibility of more economical, direct methane conversion processes. Oxidative coupling of methane over oxide catalysts is one approach currently being explored.

Keller and Bhasin[4] studied the catalytic oxidative coupling of methane to C_2 compounds over γ-Al_2O_3 supported metal oxides. Methane and oxygen were fed into the reactor cyclically to minimize competing gas-phase noncatalyzed reactions. The metal oxide catalyst undergoes a Mars–van Krevelen type mechanism[5] with the lattice oxygen participating in a redox cycle. Methyl radicals produced at the oxide surface as a result of hydrogen abstraction react to form C_2 compounds. At present, it is not entirely clear whether this reaction occurs primarily in the gas phase or at the oxide surface.

Sofranko et al. found that cyclic redox and methane/oxygen cofeed reactions over Mn/SiO_2 catalysts resulted in comparable

(1) Chamberlain, D. S.; Bloom, E. B. *Ind. Eng. Chem.* **1929**, *21*, 945.
(2) Sofranko, J. A.; Leonard, J. J.; Jones, C. A. *J. Catal.* **1987**, *103*, 302.
(3) Jones, C. A.; Leonard, J. J.; Sofranko, J. A. *Energy Fuels* **1987**, *1*, 12.
(4) Keller, G. E.; Bhasin, M. M. *J. Catal.* **1982**, *73*, 9.
(5) Mars, P.; van Krevelen, D. W. *Chem. Eng. Sci. Suppl.* **1954**, *3*, 41.

0022-3654/90/2094-0409$02.50/0

values of methane conversion (~22%) and product selectivities (~77%) to C_2 hydrocarbons under similar conditions.[3,6] Methyl radical production via H-atom abstraction is the first step of methane activation. These authors identified ethylene and higher hydrocarbons as secondary products since their selectivity increases with increasing reactor residence time.[2] Ethane was assigned as the primary product since its selectivity increased with decreasing residence time. They propose nonselective products are formed primarily by destruction of methyl radicals at low methane conversion and destruction of olefinic and aromatic products at high conversion.[6]

Lunsford et al. propose that carbon oxides are primary products formed by direct reactions of methyl radicals with surface O^{2-} ions or gaseous oxygen or via the formation and decomposition of surface methoxide ions.[7-10] This conclusion was based on experiments where methane and ethane were passed separately over Li/MgO at 620 °C. The yield of CO and CO_2 produced during methane conversion was found to be greater than that obtained with ethane by a factor of 3.6 even though ethane may easily react with surface O^- ions to produce C_2H_4, CO, and CO_2.[8]

While there is a general consensus that methane activation takes place by H-atom abstraction at the catalyst surface, there is some controversy regarding the subsequent chemistry of the radical intermediates. In general, secondary reactions, which prevail at the high temperatures used in catalytic methane activation, obscure an understanding of the gas and surface phase chemistry of radical species. Since the main technological goal is to increase hydrocarbon selectivities and decrease oxidation products, it is essential to know the mechanism and active sites for the formation of these products so that selective catalysts can be designed.

In the present study pulsed-laser-induced methane activation over oxide surfaces was employed to provide a low-temperature route to methane activation in an effort to clarify the role of surface versus gas-phase radical chemistry. Methyl and methylene radicals, two of the important reactive intermediates detected during catalytic methane activation, are produced in radio frequency discharge plasmas.[11-13] Therefore, we supposed that they may also be produced by laser-induced plasmas. It is well-known that when the light intensity and gas pressure are beyond a certain threshold, gas breakdown can be induced by a laser beam regardless of the absorption properties of the gas[14,15] and that focusing the laser beam at a solid surface lowers this threshold.[15,16] Intense plasmas are generated due to the subsequent absorption of laser light via the inverse bremsstrahlung process.[15] High-energy electrons are produced in these plasmas and electron molecule collisions lead to the formation of ions and radicals near to the surface.[15,17-19]

Pulsed laser irradiation (100 mJ at 308 nm) of oxide surfaces in a methane atmosphere led to methane activation giving both dimerization and oxidation products even in the absence of gas-phase oxygen. Based on direct observation of light emission, methane activation can be attributed to a plasma that was initiated at the oxide surface and then propagated into the gas phase. The oxides used were lithium carbonate promoted magnesia, titania, and silica. The effects of different oxides and oxide pretreatments on methane conversion and product selectivity were studied to investigate the sensitivity of product distributions to surface properties. Relatively high conversions, 7%, and C_2 selectivities, >20%, were observed for small integrated irradiation times of ~5 ms. Ethane, ethylene, acetylene, carbon monoxide, hydrogen, and C_3 hydrocarbons were observed. Photographic evidence suggested that the lifetime of the intermediates was on the order of the time interval between laser pulses (1 s), which is sufficiently long for complete thermal accommodation with the ambient gas. Heating of the oxide surface and the gas by the laser was negligible. Hydrocarbon products were formed by primary reactions of the gas-phase radicals, and carbon monoxide arises from reaction of the radicals with surface oxygen species.

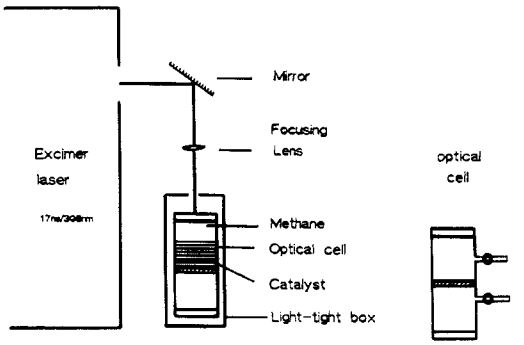

Figure 1. Optical cell and experimental setup.

Experimental Section

The apparatus for pulsed laser irradiation experiments is shown in Figure 1. Oxide powders were loaded into a gas-tight, quartz optical cell and subjected to various pretreatments. The cell was then charged with 860 Torr of methane, and the oxide powder surface was irradiated with pulses from a XeCl excimer laser (308 nm/20 ns). The laser beam was focused at or close to the oxide surface, using a 10 cm focal length lens, to produce a laser power density of ~180 MW/cm^2. Precise positioning of the laser beam focus at the oxide powder surface was difficult to achieve from run to run. However, successful positioning was indicated after a run by the appearance of carbon deposited on the surface of the oxide and the cell walls. Irradiations were carried out with the cell at 300 K for 3 h at a repetition rate of 25–35 Hz (~300 000 pulses). All irradiation experiments were performed under the stated conditions of pressure, temperature, laser-oxide surface geometry, pulse energy, and pulse number unless specified otherwise.

The gas composition was determined before and after laser irradiation by using a VG Instruments SX200 quadrupole mass spectrometer. The partial pressure of each product, ethane, ethylene, acetylene, and carbon monoxide, was determined relative to the partial pressure of methane by comparison to standards made up of equimolar mixtures of the pure compounds. The partial pressure of ethane in the irradiated gas was evaluated according to

$$P_{C_2H_6} = \frac{\mathrm{IS(16\ amu)}}{\mathrm{IS(30\ amu)}} \frac{\mathrm{IM(30\ amu)}}{\mathrm{IM(16\ amu)}} P_{CH_4}$$

where IS( ) is the intensity at the indicated charge to mass ratio in the standard mixture and IM( ) is the measured increase in intensity from the experiment. Mass spectral determination of the ethylene partial pressure includes a correction due to the contribution from C_2H_6 fragmentation at 27 amu

$$P_{C_2H_4} = \frac{\mathrm{IS(16\ amu)}}{\mathrm{IS(27\ amu)} - R(C_2H_6)\ \mathrm{IS(30\ amu)}} \times \frac{\mathrm{IM(27\ amu)} - R(C_2H_6)\ \mathrm{IM(30\ amu)}}{\mathrm{IM(16\ amu)}} P_{CH_4}$$

where $R(C_2H_6) = I(27\ \mathrm{amu})/I(30\ \mathrm{amu})$ measured for pure ethane. Similar formulas were employed to determine the partial pressures of acetylene and carbon monoxide relative to methane.

(6) Jones, C. A.; Leonard, J. J.; Sofranko, J. A. *J. Catal.* **1987**, *103*, 311.
(7) Ito, T.; Lunsford, J. H. *Nature* **1985**, *314*, 721.
(8) Ito, T.; Wang, J.-X.; Lin, C.-H.; Lunsford, J. H. *J. Am. Chem. Soc.* **1985**, *107*, 5062.
(9) Aika, K.-I.; Lunsford, J. H. *J. Phys. Chem.* **1977**, *81*, 1393.
(10) Driscoll, D. J.; Martir, W.; Wang, J.-X.; Lunsford, J. H. *J. Am. Chem. Soc.* **1985**, *107*, 58.
(11) Smolinsky, G.; Vasile, M. J. *Int. J. Mass Spectrom. Ion Phys.* **1975**, *16*, 137.
(12) Vasile, M. J.; Smolinsky, G. *Int. J. Mass Spectrom. Ion Phys.* **1975**, *18*, 179.
(13) Hiraoka, K.; Aoyama, K.; Morise, K. *Can. J. Chem.* **1985**, *63*, 2899.
(14) Kojima, J.; Naito, K. *Ind. Eng. Chem. Prod. Res. Dev.* **1981**, *20*, 396.
(15) Ready, J. F. In *Effects of High-Power Laser Radiation*; Academic Press: New York, 1971.
(16) Graf, H. P.; Kneubuhl, F. K. *Appl. Phys.* **1983**, *B31*, 53.
(17) Graf, H. P.; Kneubuhl, F. K. *Helv. Phys. Acta* **1981**, *54*, 290.
(18) Winters, H. F. *J. Chem. Phys.* **1975**, *63*, 3462.
(19) Manton, J. E.; Tickner, A. W. *Can. J. Chem.* **1960**, *38*, 858.

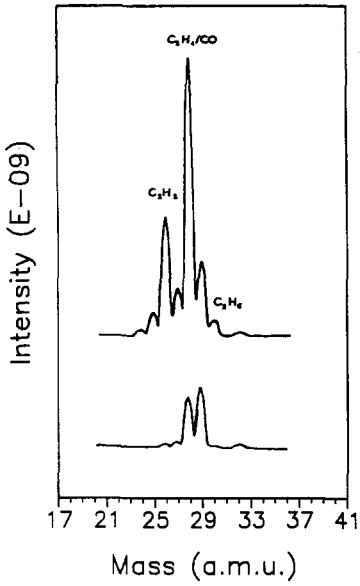

Figure 2. Mass spectra in the C_2 region (lower) before and (upper) after pulsed laser irradiation of Li/MgO in a CH_4 atmosphere indicating an increase in the peak intensities at 26, 28, and 30 amu corresponding to C_2H_2, C_2H_4/CO, and C_2H_6.

Methane conversion and selectivity to products were calculated from partial pressures, with C_2 product partial pressures multiplied by 2 and assuming conservation of gas-phase carbon, i.e. conversion to adsorbed carbon species is neglected

$$\text{conversion (\%)} = \frac{\text{sum of the product partial pressures}}{\text{initial methane pressure}} \times 100$$

$$\text{selectivity (\%)} = \frac{\text{partial pressure of } x}{\text{partial pressure of total products}} \times 100$$

Oxide Preparation

Li_2CO_3, LiOH, and MgO were purchased from Fisher Scientific Co. (certified ACS), TiO_2 from Aldrich Chemical Co. (99.9%), and SiO_2 from Davison Chemical Specialty Co. (grade 953). CH_4 and O_2 (99% pure) were purchased from Matheson Gas Co. and $^{13}CH_4$ and CD_4 (99.7 atom % deuterium) from Isotec, Inc. All gases were used without further purification.

Lithium promoted oxide powders (7 wt %) were prepared by adding requisite amounts of Li_2CO_3 and the supporting oxide (MgO, TiO_2, or SiO_2) to deionized water. The mixture was heated with stirring to a thick paste and dried at 413 K for more than 24 h.

Prior to irradiation, oxide powders were subjected to a variety of pretreatments. All oxides were precalcined in flowing oxygen (50 mL/min) in a quartz reactor at 723 K for 2.5 h and then ground in air and transferred to the optical cell (designated as the standard pretreatment or std). The oxide powder was used in x irradiation runs (designated as the experimental treatment or expt) and reoxidized in the optical cell under the standard oxidation conditions (designated as reox). The optical cell containing the precalcined oxide was evacuated without heating (designated as evac) or evacuated at 473–523 K for 1–2 h (designated as evac with heating).

Results and Discussion

Laser-Induced Methane Activation. Initially, methane gas (860 Torr) was subjected to the standard irradiation at 300 K, in the absence of oxide powder. Methane activation was not observed as evident by the absence of dimerization or oxidation products. Methane activation was observed when lithium promoted magnesium oxide (std + evac) was irradiated in a methane atmosphere under standard experimental conditions. Figure 2 shows mass spectra in the C_2 region taken before and after irradiation. An increase in the peak intensities at 26, 28, and 30 amu corresponding to the major peaks of acetylene, ethylene/CO, and ethane are clearly visible. The peak at 29 amu is due to a background impurity.

TABLE I: Methane Conversion and Product Selectivities over 7 wt % Li/MgO Oxide Powder after Pulsed Laser Irradiation

powder treatment	% conversion	% product selectivity				
		C_2H_6	C_2H_4	C_2H_2	C_2	CO
1. evacuated	6.9	16	2.2		18.2	81.8
2. expt + evac	7.0	22.6		0.5	23.1	76.9
3. reoxd + evac with heating	5.6	18.6		0.04	18.6	81.4
4. evac with heating	6.86	16.4	1.6	3.8	21.8	78.2
5. expt + evac	6.0	26	6.5	1.1	33.6	66.4
6. expt + evac	5.33	21.6	11	5.8	38.4	61.6

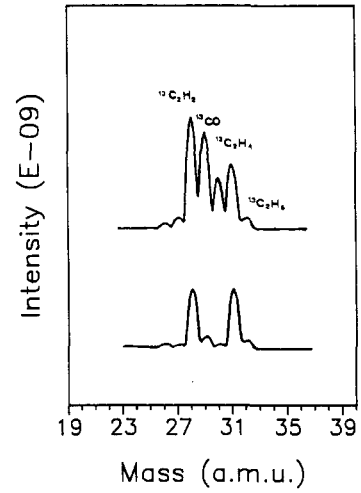

Figure 3. Mass spectra in the C_2 region (lower) before and (upper) after pulsed laser irradiation of Li/MgO in a $^{13}CH_4$ atmosphere indicating an increase in the peak intensities at 28, 29, 30, and 32 amu corresponding to $^{13}C_2H_2$, ^{13}CO, $^{13}C_2H_4$, and $^{13}C_2H_6$, respectively.

Table I exhibits data for methane conversion and product selectivity determined for a series of pulsed laser irradiation experiments over Li/MgO. The experiments were carried out with the laser focus at the oxide surface as identified by the large amount of carbon deposited. Conversions for different oxide pretreatments were reproducible within ±2%. Methane conversion calculations do not account for deposited carbon, as total conversion values are higher than those reported. The conversions are high compared to high-temperature, catalyzed reactions considering that the integrated irradiation time (equivalent to the contact time in a catalytic flow reactor) during a typical experiment was only ~5 ms. The major product was CO even though the experiments were carried out in the absence of gas-phase oxygen. This indicates that the oxygen in CO is extracted from the oxide. No carbon dioxide was detected consistent with the absence of secondary reactions of CO. Significant amounts of C_2 products were formed including ethane, ethylene, and acetylene. Ethane was the major C_2 product and ethane selectivities, ~20 ± 5%, were much greater than ethylene and acetylene selectivities (1–10%). The rate of dimer formation was evaluated as 6×10^{17} molecules/cm^3 per second of irradiation time or 1×10^{10} molecules/cm^3 per laser shot.

After irradiation, the oxide powder (top 3–4 mm layer) appeared gray-black and a black powder coated the cell walls. This black deposit was due to deposited carbon. The carbon was removed by heating to 723 K in flowing oxygen (10 mL/min) to form CO and CO_2, which were identified by gas chromatography.

Since the yield of products is low, experiments were carried out to check for various artifacts such as product formation by decomposition of Li_2CO_3 or by reaction of carbon impurities on the surface of the oxide powder. To rule out these possibilities, irradiation experiments were performed using isotopically labeled $^{13}CH_4$ in order to trace the origin of the carbon in the observed products. $^{13}CH_4$ gas (1070 Torr) was irradiated under standard experimental conditions over the Li/MgO powder. Figure 3 shows

mass spectra in the C_2 region measured before and after an irradiation experiment. The spectra differ considerably from those in Figure 2. Peaks at 28, 29, 30, and 32 amu indicate the formation of $^{13}C_2H_2$, ^{13}CO, $^{13}C_2H_4$, and $^{13}C_2H_6$, respectively. The peak at 31 amu is due to a background impurity. The results prove that dimerization and oxidation products arise primarily from methane activation.

Laser-induced activation of methane occurs in a plasma initiated at the surface of the oxide powder. Evidence for plasma formation has been obtained via observation of light emitted by the plasma. Figure 4a is a photograph of the emission produced by the laser focused on the oxide surface in a methane atmosphere (2 s exposure + 16 Hz laser repetition rate = 32 pulses recorded). Emission is clearly visible both along the path of the converging laser beam and from the point where the beam strikes the oxide powder surface. When the cell was evacuated only emission from the oxide surface was observed; there was no emission along the beam path in the volume above the oxide surface. No emission of any kind was observed in the absence of oxide powder even with a methane atmosphere present in the cell.

It is well-known that methane plasmas may be produced by laser irradiation as well as by electrical/microwave/radio frequency (rf) discharges in the gas phase.[13,15,20-23] The mechanism of laser-induced plasma formation has been described in detail. Plasmas initiate with the emission of free electrons in the gas phase.[15] Electron emission results from laser-surface interactions[24] such as thermionic emission from surface defects,[15,23,24] multiphoton photoelectric effects,[15] or enhanced electric fields at surface protrusions.[23,25] The electrons are accelerated by absorption of energy from the laser beam via the inverse Bremsstrahlung process.[15] Collisional ionization of gas-phase molecules leads to additional low-energy electrons ultimately causing an avalanche of ions and electrons. During this process, electrons absorb sufficient energy to dissociate methane molecules to produce a variety of radicals and ions which react to form the observed products. The model of electron-induced methane dissociation is supported by results from experiments on the decomposition of methane using low-energy electrons.[18,19] The product distribution observed in the latter experiments was similar to that obtained here.

Several alternative mechanisms for laser-induced methane activation can be eliminated from consideration namely, gas-phase photolysis, high-temperature pyrolysis, and thermal catalysis. Direct photolysis can be ruled out since methane does not absorb at 308 nm. Gas-phase pyrolysis is ruled out by the lack of any methane conversion in the absence of MgO powder. The possibility of thermal catalysis can be eliminated by consideration of the temperature rise produced by the focused laser. By means of a simple calculation described in Appendix 1, the temperature of MgO particles is estimated to rise only 69 K. Under the existing experimental conditions (contact time, 5 ms; irradiated area, 0.01 cm^2; the absence of gas-phase oxygen and low surface temperature rise), thermal catalysis is eliminated.

The important reactive intermediates present in our experiments, $^{\bullet}CH_x$ ($0 \leq x \leq 3$), can be inferred from studies of rf discharges and laser-induced plasmas reported in the literature. First, the product distribution obtained in rf discharges has been shown to be a strong function of the input power.[20-22] Acetylene and hydrogen were the major products obtained at high input powers.[20] At low input powers, ethane, ethylene, and acetylene were produced in comparable amounts.[20,21] The product distributions obtained at high input laser powers [a few GW/cm^2], mainly acetylene and hydrogen,[15,26] and at the low input powers used in the present experiments also exhibit similar trends. This similarity in product distributions suggests that the chemistry in rf discharges and laser-induced plasmas is similar. Second, although both radicals and ions are present in discharges, Gevantmann and Williams,[27] using iodine as a free radical scavenger, concluded that methyl, methylene, and ethyl radicals were the important intermediates in the decomposition of methane by high-energy

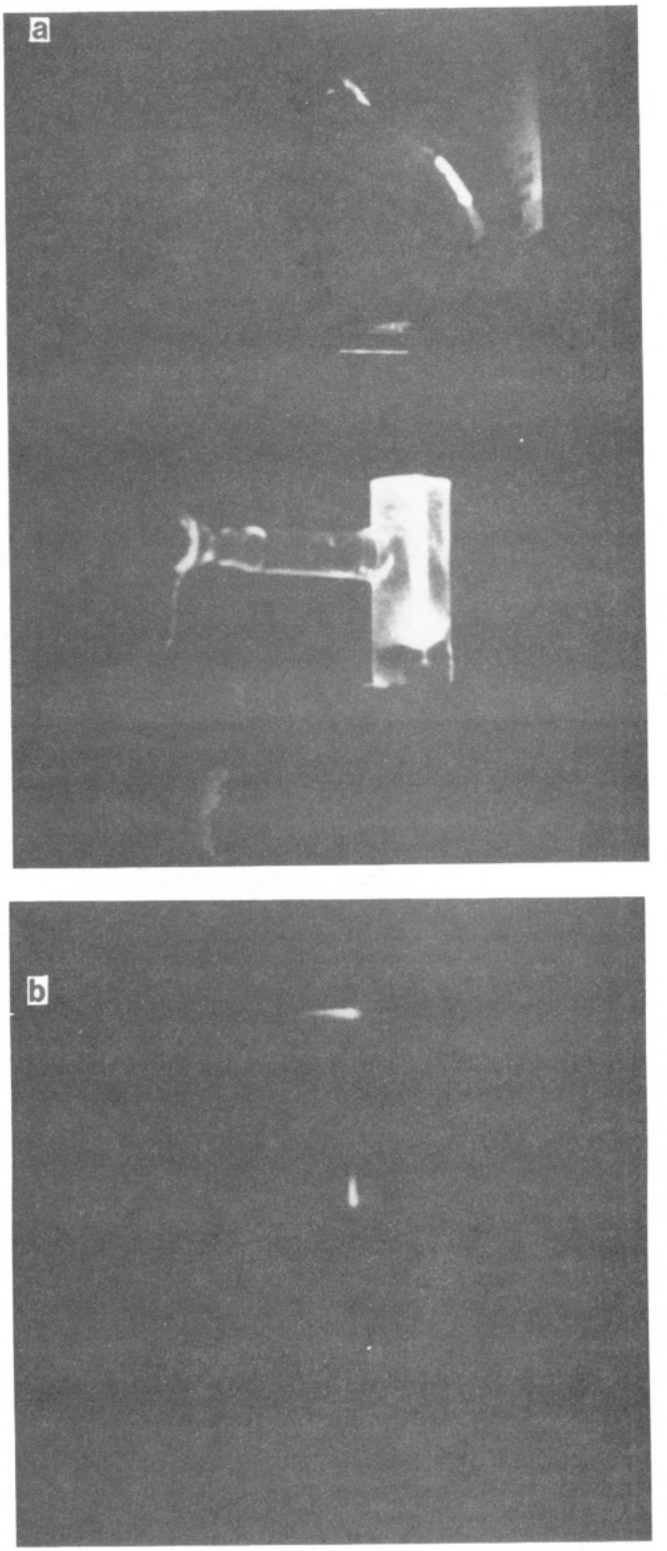

Figure 4. (a) Plasma emission and propagation in a cell with Li/MgO oxide and methane gas (2000 ASA, 32 laser pulses). (b) Plasma emission and propagation in a cell with Li/MgO oxide and methane gas (2000 ASA, 1 Hz).

(20) Venugopalan, M.; Roychowdhury, K. C.; Pool, M. L. *Plasma Chemistry of Fossil Fuels* **1980**, *90*, 1.
(21) Vasile, M. J.; Smolinsky, G. *Int. J. Mass Spectrom. Ion Phys.* **1975**, *18*, 179.
(22) Kawahara, Y. *J. Phys. Chem.* **1969**, *73*, 1648.
(23) Smith, D. C. *J. Appl. Phys.* **1977**, *48*, 2217.
(24) Walters, C. T. *Appl. Phys. Lett.* **1974**, *25*, 696.
(25) Bloembergen, N. *Appl. Opt.* **1973**, *12*, 661.
(26) Graf, J. P.; Sigrist, M. W.; Kneubuhl, F. K. *Helv. Phys. Acta* **1979**, *52*, 56.
(27) Gevantmann, L. H.; Williams, R. R. *J. Phys. Chem.* **1952**, *56*, 569.

TABLE II: Effect of Laser Focus–Oxide (Li/MgO) Surface Distance or Power Density on Methane Conversion and C_2 Selectivities

laser focus–oxide surface distance, mm	power density, MW/cm^2	% conversion	% selectivity			
			C_2H_6	C_2H_4	C_2H_2	CO
0	180	6.86	16.4	1.6	3.8	78.2
−2	150	6.51	20.5	14	28	39
10	60	0.36	26.2	9.1	10	55.1

X-rays and electrons. Hiraoka et al.,[13] also employing radical and ion scavengers, showed that radical processes were mainly responsible for the products formed by radio frequency glow discharge decomposition of methane. In particular, they concluded that CH_2, CH, and C were the primary radicals produced in a methane plasma.

Pulsed laser irradiation experiments of $CH_4 + CD_4$ mixtures were carried out in order to obtain evidence concerning the identity of the radicals formed. Mixtures of $CH_4 + CD_4$ in the ratios 2:1 were irradiated over Li/MgO at a total pressure of 940 Torr under standard experimental conditions. The hydrogen–deuterium exchange rate was of the order of 10^{20} molecules/cm^3 per second of irradiation time which is 10^3 times faster than the rate of dimerization/oxidation. The observation of CH_3D and CD_3H is consistent with methyl radical formation. D_2 and D_3 compounds are formed indicating CH_2 radicals may also be produced. The formation of C_2H_4, C_2D_4, C_2H_2, and C_2D_2 also supports the production of methylene radicals. Thus, CH_4–CD_4 exchange experiments give evidence for the formation of CH_3 and CH_2 radicals.

The emission from the volume above the oxide surface in the path of the incident laser beam is noteworthy. Ramsden and Davies[28] reported that laser-induced plasmas propagate back along the direction of the incident laser beam at a velocity of $\sim 10^7$ cm/s. This phenomenon has been described as a radiation-supported shock wave.[29] However, it is unlikely that the emission observed in our experiments is due to this effect. The emission shown in Figure 4a extends approximately 5 cm above the focal point at the oxide surface. A propagation velocity of $\sim 10^9$ cm/s would be required for the plasma to expand 5 cm during the laser pulse. Alternatively, the emission may be caused by laser-excited fluorescence of gas-phase species. Since neither methane nor any of the stable products absorb at the incident laser wavelength, the emission could be due to laser-excited fluorescence of radical intermediates. The half-lives of candidate radical species were calculated from the pseudo-first-order rate constants of their reactions with methane.[30-32] The half-lives of CH and C_2 radicals were 8.34×10^{-11} and 1.34×10^{-9} s, respectively, which indicates they do not live long enough to absorb radiation and fluoresce. The CH_2 radical has a half-life 0.011 s; however, it has a very weak absorption in the near-ultraviolet ($a\ ^1A_1 \rightarrow c\ ^1A_1$).[33] This combination of a relatively short lifetime and weak absorption makes it unlikely that CH_2 is the species responsible for fluorescence in the laser irradiation experiments. CH_3 radicals do not absorb at 308 nm.[33] The emission is most likely due to ions and electrons in a low-density plasma which absorb in a nonspecific manner and emit in the visible region.

This mechanism of gas-phase emission has important implications for the lifetime of gas-phase species under our experimental conditions, namely the emitting species must persist during the time interval between laser pulses. As seen in Figure 4b the gas-phase emission is observable for laser pulse repetition rates of only 1 Hz, which implies that the intermediates persist for times of the order of 1 s.

TABLE III: Effect of Pretreatment on Methane Conversion and C_2 Selectivity over Li/MgO (7 wt %)

powder pretreatment	% conversion	% product selectivity	
		C_2	CO
reoxd + evac	11.6		100
reoxd + evac	1.04	2.3	97.7
reoxd + evac with heating	4.4	32.2	67.8
reoxd + evac with heating	5.6	18.6	81.4

Laser power density at the oxide surface has a strong influence on methane conversion. Table II summarizes the conversions and product selectivities for three different laser focus/oxide surface geometries: 0 corresponds to the laser focus at the oxide surface; −2 corresponds to the laser focus 2 mm below the oxide surface; and 10 corresponds to the laser focus 10 mm above the Li/MgO (reoxd and evac with heating) oxide surface. Power densities are calculated from the focusing geometry. Methane conversion increases with power density. This increase in conversion may be attributed to higher electron densities and a corresponding increase in the number of electron–molecule collisions. Carbon deposition was not detected at the low power densities (60 MW/cm^2). At higher power densities ($\sim$180 MW/cm^2), a large amount of carbon is formed. CO was the major product detected at all power densities. Since conversion and product selectivity are a strong function of the focusing geometry, care was taken to carry out the experiments with the laser beam focused tightly on the oxide surface.

Radical–Surface Interactions. Since laser-induced methane activation produces mainly CH_3 and CH_2 radicals in the gas phase, this technique may be utilized to study the interaction of radical species with a catalyst surface. The oxide surface temperature rise during these reactions has been calculated to be very low, $\sim$70 K. Therefore, the technique makes it possible to investigate the chemistry of the radical species both in the gas phase and at the oxide surface in the absence of secondary reactions and at room temperature. For example, the effect of different oxides and oxide pretreatments on methane conversion and product selectivity indicates whether the reactions leading to the formation of products are surface sensitive.

The influence of oxide pretreatment on conversion and selectivity was investigated for Li/MgO. The results summarized in Table I indicate that conversion and selectivity are relatively insensitive to the various pretreatments listed. However, a pronounced pretreatment effect is observed when oxide samples are reoxidized in the optical cell depending upon the sample temperature during evacuation after reoxidation. The results are summarized in Table III. CO selectivity is increased and C_2 selectivity suppressed for reoxidized samples evacuated at room temperature compared to reoxidized samples evacuated at 473–523 K. The increase in CO selectivity must be due to the presence of reactive surface oxygen species after reoxidation which are removed by evacuation at elevated temperatures. Thus, the surface reactivity appears to be a strong function of the nature of oxygen species on the surface. Although the focusing geometry may effect the conversions, such high CO product selectivities were not observed for experiments where the oxides were evacuated with heating after reoxidation. Furthermore, the results in Tables II and III strongly suggest that CO is a primary product formed by the reaction of radical intermediates with surface oxygen on the oxide powder. If CO were a secondary product, the CO selectivity would decrease with decreasing conversion which is not the case.

Laser-induced activation experiments were also carried out over lithium promoted and unpromoted MgO, TiO_2, and SiO_2. Figure 5 shows the methane conversion and selectivity behavior for the different oxides. The fact that methane activation is observed over different surfaces including the unpromoted oxides is consistent with the plasma mechanism. In order to eliminate the effects of focusing geometry on conversion and product selectivity,

(28) Ramsden, S. A.; Davies, W. E. R. *Phys. Rev. Lett.* **1964**, *13*, 227.
(29) Ramsden, S. A.; Savic, P. *Nature* **1964**, *203*, 1217.
(30) Dobe, S.; Bochland, T.; Temps, F.; Wagner, H. G. *Ber. Bunsen-Ges. Phys. Chem.* **1985**, *89*, 432.
(31) Butler, J. E.; Ross, L. P.; Sin, M. C.; Hudgens, J. W. *Chem. Phys. Lett.* **1979**, *63*, 104.
(32) Pasternack, L.; McDonald, J. R. *Chem. Phys.* **1979**, *43*, 173.
(33) Herzberg, G. In *Molecular Spectra and Molecular Structure. III. Electronic Spectra and Electronic Structure of Polyatomic Molecules*; D. Van Nostrand Company, Inc.: London, 1966.

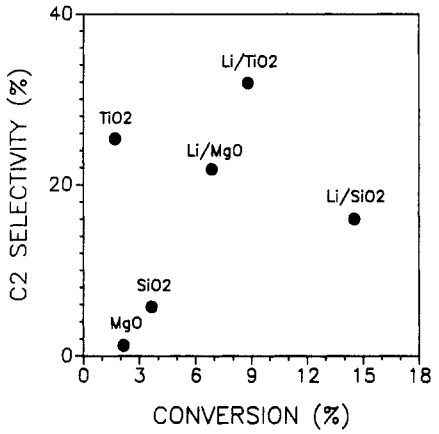

Figure 5. Methane conversions and C_2 product selectivities determined for pulsed laser irradiation experiments over MgO, TiO_2, SiO_2, Li/MgO, Li/TiO_2, and Li/SiO_2.

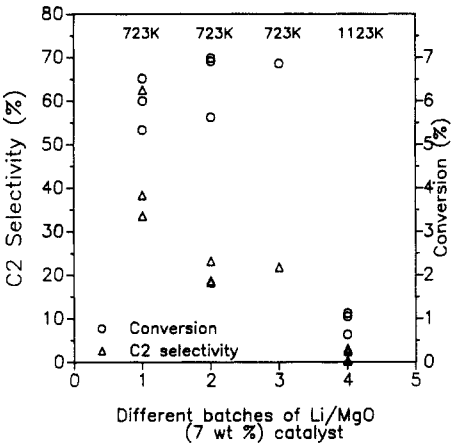

Figure 6. Methane conversions and C_2 product selectivities determined after pulsed laser irradiation experiments for four different batches of Li/MgO (7 wt %) catalyst precalcined at 723 and 1123 K, respectively.

each data point is a representation of several experiments. The change in methane conversion for the different oxides may be due to (1) different electron emission and vaporization properties of the materials influencing the expansion, temperature, and density of the plasma or (2) radical–oxide surface interactions resulting in different product distributions and methane conversions. The lithium promoted oxides exhibit higher conversions compared to the unpromoted oxides. This may be due to enhanced electron emission associated with low work function lithium surface phases leading to higher plasma density. MgO and SiO_2 exhibit low C_2 selectivities as compared to the other oxides. Radical–oxide surface reactions are likely responsible for this behavior.

Further experiments were carried out to investigate the effect of oxide pretreatment on the product distribution. Different batches of Li/MgO were precalcined at different temperatures. The three batches precalcined at 723 K give fairly reproducible values of methane conversion and selectivity for a series of runs as shown in Figure 6. However, the sample calcined at 1123 K exhibits extremely low conversion and C_2 selectivity similar to unpromoted MgO. This result supports the idea that surface–radical reactions play an important role in determining final product distributions. The surface contribution probably arises through radical adsorption on oxide surfaces when radicals interact with oxygen or hydroxyl species. The difference in conversion obtained at a higher calcination temperature may be due to an increase in the work function of the oxide.

Conclusions

Pulsed laser irradiation of oxides in a methane atmosphere led to methane activation. Methane activation was attributed to plasma formation based on direct photographic evidence and comparison of product distributions with the literature. CH_3 and CH_2 radicals are produced in the plasma as a result of electron molecule collisions in the gas phase. Since the surface temperature rise is very low, 69 K, high-temperature secondary reactions are not important for these experiments. This process is thus utilized to investigate the surface sensitivity of radical reactions.

CO was the major product observed at room temperature, in the absence of gas-phase oxygen, and at very low power densities. This indicates (1) oxygen is extracted from the oxide catalyst through radical–oxide surface reactions and (2) CO is a primary product of the reaction between the CH_3/CH_2 radicals and surface oxygen species. These results agree with those of Lunsford et al.[7-10] who propose that carbon oxides are primary products formed by direct reactions of CH_3 radicals with surface O^{2-} ions or gaseous oxygen or via the formation and decomposition of surface methoxide ions. Ethane, ethylene, and acetylene must be primary products based on the similarity in selectivity between these experiments and rf discharge results. Furthermore, acetylene is observed at low power densities, room temperature, and low conversions where the opportunities for secondary reactions of ethane and ethylene are minimized. Carbon formation increases at high laser power densities as a result of high-energy electron–molecule collisions.

Since methyl and methylene radicals are produced at low temperatures, competing gas-phase secondary reactions are eliminated. Thus the steps involving product formation may be studied at room temperature which is not possible in thermal catalytic reactions due to the high temperatures involved. The surface sensitivity of these reactions is detected through the changes in conversion and selectivity as a function of different oxides and oxide pretreatments. The experiments clearly indicate that oxidation of the catalyst strongly influences the CO/C_2 product selectivities indicating enhanced methyl radical–oxide oxygen reactions. Conversions and product selectivities are also strongly influenced by the oxides used. These results imply that radical–oxide surface reactions are important even at room temperature in determining the product selectivities. However, further information regarding gas-phase or surface contributions of these reactions could not be obtained since the surface is also involved in the methane activation process. Hence, another set of experiments was carried out where the CH_3 radicals are produced in the gas phase via azomethane photolysis and then allowed to interact in the gas phase and with the oxide surface. These results will be presented in another paper.

Acknowledgment. We gratefully acknowledge the financial support of the Amoco Corporation through the University Methane Research Program.

Appendix 1

The maximum surface temperature rise was calculated for MgO particles at the focus of a laser beam by calculating the energy absorbed by a particle and assuming no heat losses. For the sake of simplicity the particles are taken to be cubic so that the maximum temperature rise is given by

$$\Delta T = \frac{E(l^2/A)(1 - e^{-kl})}{C_{p,m}(\rho l^3/M)}$$

where E is the laser pulse energy (100 mJ), l is the dimension of a cubic MgO particle, A is the area of the laser beam at the focus (1×10^{-4} cm^2), k is the absorption constant (2.3 cm^{-1}) obtained from transmission curves[34] by application of the Beer–Lambert law, $C_{p,m}$ is the molar heat capacity of MgO (37.5 J/(K mol)), ρ is the density of MgO (3.58 g/cm^3), and M is the molar mass of MgO (40 g/mol). For l in the range characteristic of the powders used for the laser irradiation experiments, 10^{-4} to 10^{-2} cm, the maximum temperature rise is essentially constant at ~69 K.

Registry No. CH_3, 2229-07-4; CH_2, 2465-56-7; SiO_2, 7631-86-9; Li, 7439-93-2; MgO, 1309-48-4; CH_4, 74-82-8; TiO_2, 13463-67-7.

(34) Kodak publication U-72, "Kodak IRTRAN Infrared Optical Materials".